Supporting Information

Facile synthesis of Co-based catalysts with high dispersion via an eco-Friendly strategy

Feng Gu, [a] Guoqing Xiao,[a] Qiuyao Jiao, [a] Yan Liu, [b,*] Pengyong Wei [a] and Lei Li [a,*]

[a] *School of Chemistry and Chemical Engineering, Yancheng Institute of Technology, Yancheng, 224051, PR China*

[b] *State Key Laboratory of Coal Conversion, Institute of Coal Chemistry, Chinese Academy of Sciences, Taiyuan 030001, Shanxi, PR China*

Corresponding Authors

E-mail: lee_ycit@hotmail.com (L. Li), liuyan@sxicc.ac.cn (Y. Liu).

1. Experimental Section

1.1 Characterizations

Powder X-ray diffraction patterns of samples were recorded on a Rigaku Miniflex-600 operating at 40 kV voltage and 15 mA current with CuKα radiation (λ=0.15406nm). N_2-adsorption desorption characterization was conducted on an ASAP 2460 (America, Micromeritics) instrument. Each sample (0.1 g) was degassed by vacuum treatment at 573 K for 4 h. After physically adsorbed water and impurities were removed, the textural properties were obtained at 77 K. The surface area and pore diameter were calculated by the BET and BJH methods, respectively.

Transmission electron microscopy (TEM) was carried out by a JEM-2100F FETEM equipped with energy dispersive X-ray spectrometer (EDX) analyses at 100 kV, and EDX elemental mapping were operated at 200 kV.

The X-ray photoelectron spectroscopy (XPS) measurements were performed on a multifunctional imaging electron spectrometer (VG, ESCALAB 250XI, Thermo Scientific, Surrey) with Al Kα (hν = 1486.6 eV) radiation. Corrections to the sample data were carried out by setting the binding energy of adventitious carbon (C 1s) at 284.8 eV. The XPS fitting was performed by XPS peak software. After opening data, the background type is chose Shirley. According to standard value of different chemical value of Co, the initial peaks were added sequentially. In this process, the constrains were used, such as % Lorentzian-Gaussian was set as 80%, and the peak area ratio between $2P_{3/2}$:$2P_{1/2}$ was set as 2:1. Finally, the fitting was optimized.

Hydrogen temperature programmed reduction (H_2-TPR) was carried out using a

Micromeritics Autochem II 2920 apparatus. All the investigated samples (50 mg) were pretreated at 300 °C for 1 h in Ar to remove impurities adsorbed on the surface before measurement.

For H_2-TPD characterization, 30 mg catalyst was reduced in pure H_2 (30 mL/min) at 673 K for 5 h. Then, 10 % H_2/Ar (30 mL/min) gas was introduced when the bed temperature decreased to 323 K. After maintaining at this temperature for another 1 h, the pure Ar gas was (30 mL/min) switched. Then, the TCD signal could be recorded after the baseline was stabilized. Finally, the H_2-TPD patterns were collected after the bed temperature increased to 673 K at a rate of 10 K/ min and maintained at this temperature for 1 h. The number of active sites (superficial metallic cobalt atom) estimated from the H_2 uptakes speculating that Co/H = 1. The TOFs of different catalysts were determined from the cobalt-specific activity (A) and the dispersion of catalysts (D) using the following: $TOF=58.93\times A\times D^{-1}$.

The CO-TPD experiment is consistent with H_2-TPD experiment. After cooling to 45 ℃, switch to 5CO/95He (V/V) adsorption saturation, then switch to He blowing to remove weakly adsorbed and gas-phase CO, and finally program heating to 700 ℃ for desorption. The exhaust gas is detected by TCD and quadrupole mass spectrometry (MS), the CO signals are recorded.

Fourier transform infrared (FTIR) spectroscopy was conducted on a Bruker Tensor 27 equipped with a diffuse reflectance chamber and a liquid nitrogen detector. Prior to the experiment, the samples were reduced by a 10% H_2/Ar mixed gas at 400 °C for 6 h in a fixed-bed reactor. Following sample loading in the diffuse reflectance cell, CO

reaction gas was introduced for 30 min. After purging by Ar for 10min, the catalyst surface was analyzed.

1.2 Catalytic performance

The FTS performance of these catalysts was conducted on a stainless-steel fixed-bed reactor (inner diameter = 8 mm). Typically, the catalyst (1mL, 40 ~ 60 mesh) was diluted with quartz sand (2.5 g, 40 ~ 60 mesh) to avoid the hot point in the reactor. Before each reaction, all the catalysts were reduced in a pure H_2 atmosphere (GHSV = 6 $L \cdot h^{-1} \cdot g^{-1}$) at 400 ^oC for 10 h. Then, syngas was introduced (H_2/CO = 2/1 (v/v), GHSV = 1000 h^{-1}) after the bed temperature decreased to 373 K with the reactor pressure increasing to 2 MPa. N_2 was used as an internal standard to calculate the CO conversion and selectivity. The FTS results were calculated after the bed temperature slowly increased to 210 ^oC. Liquid products and wax were gathered through a cold trap and a hot trap (110 ^oC) respectively. The effluent gases were analyzed on a GC-2010 chromatographs of Shimadzu by using a Carbosieve-packed column equipped with a thermal conductivity detector (TCD) and a Porapak-Qcolumn equipped with a flame ionization detector (FID). N_2 with a volume ratio of 5% was mixed in the synthetic gas. To ensure the reliability of the data, the data were obtained after a steady state time on stream of 48 h with carbon balance, nitrogen balance and total mass balance in the range of 100 ± 5%. On a molar carbon basis, oxygenates were less than 1% of the product distribution.

Supplementary tables and figures

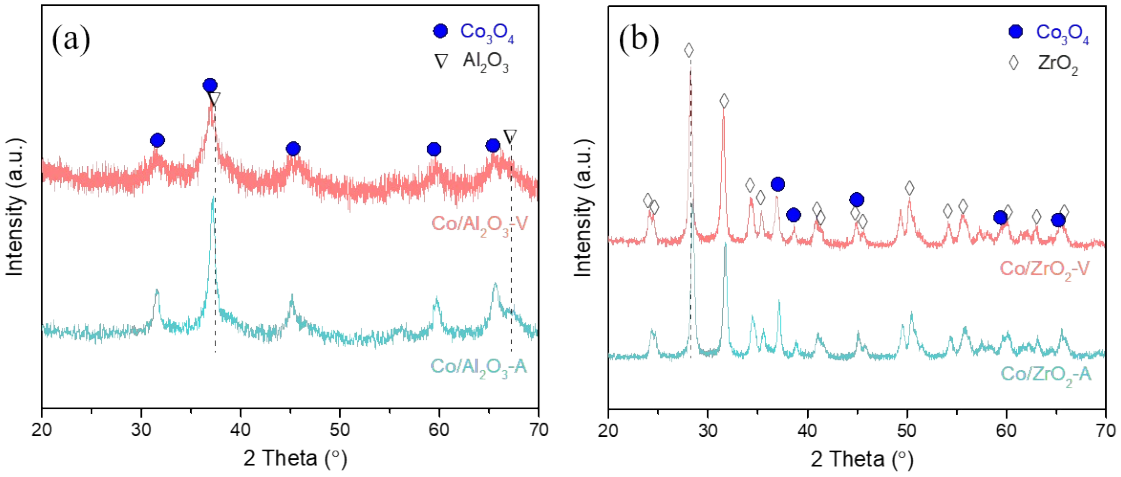

Fig. S1. XRD profiles of (a) Al_2O_3 supported Co catalysts and (b) ZrO_2 supported Co catalysts.

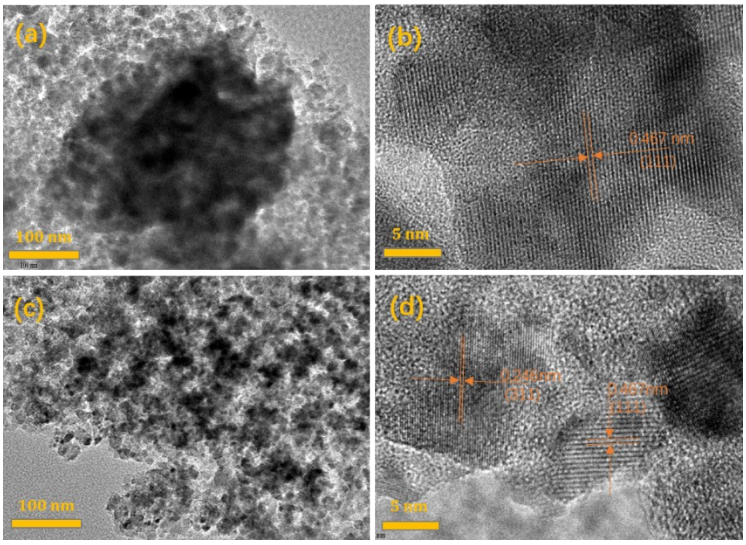

Fig. S2. HRTEM images of different catalysts, (a, b) Co/SiO_2-A and (c, d) Co/SiO_2-V.

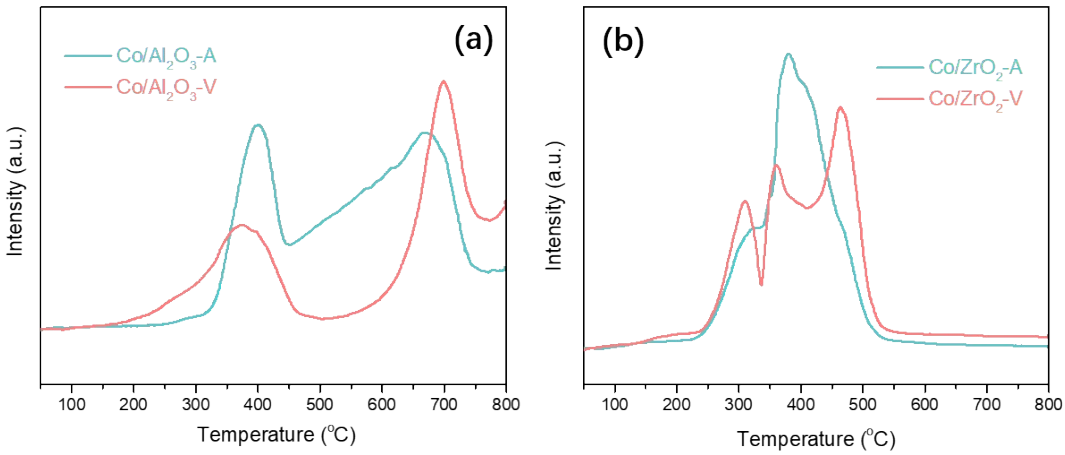

Fig. S3. H_2-TPR profiles of Co/Al_2O_3 (a) and (b) Co/ZrO_2 samples.

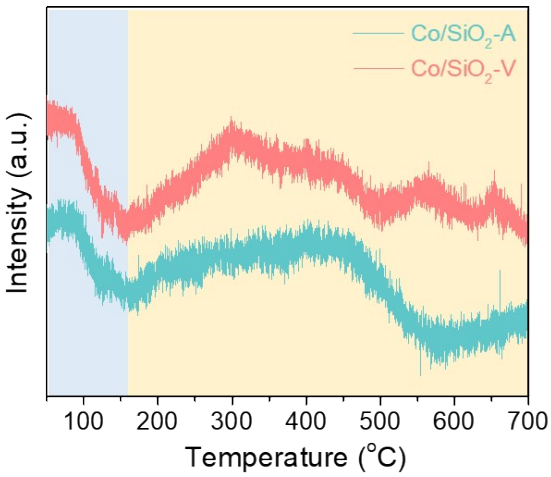

Fig. S4. CO signals of CO-TPD of different Co/SiO_2 samples.

Table S1 Phys-chemical properties of different catalysts.

Sample	S_{BET} (m^2/g)	Pore volume (cm^3/g)	Pore size (nm)	$d(Co_3O_4)^a$ (nm)	$d(Co_3O_4)^b$ (nm)
Co/SiO_2-A	140.9	0.61	17.4	18.3	20.1
Co/SiO_2-V	135.6	0.60	17.7	11.7	9.6
Co/Al_2O_3-A	143.15	0.38	10.6	13.9	12.9
Co/Al_2O_3-V	141.68	0.39	11.0	10.5	8.9
Co/ZrO_2-A	24.1	0.12	20.9	19.0	21.1
Co/ZrO_2-V	29.0	0.16	22.2	17.5	20.3

[a] the mean particle size of Co_3O_4 calculated from XRD diffraction peak at 36.8◦.

[b] the mean particle size of Co_3O_4 calculated from all XRD diffraction peaks through JADE software.

Table S2 XPS results of different Co/SiO_2 catalysts.

Sample	Surface atomic (at.%)			Co/Si ratio	$Co2p_{3/2}$BE (eV)		Co^{2+}/Co^{3+}
	Si	Co	O		Co^{3+}	Co^{2+}	
Co/SiO_2-A	31.84	1.22	62.95	0.04	780.23	781.7	0.81
Co/SiO_2-V	31.18	2.42	61.40	0.08	780.48	782.19	0.96

Table S3 Catalytic performance of Al_2O_3 and ZrO_2 supported cobalt catalysts.

Catalyst	Conv. (CO)[a]/%	S(CH_4)/%	S(C_2-C_4)/%	S(C_{5+})/%
Co/Al_2O_3-A	27.44	9.49	9.05	81.45
Co/Al_2O_3-V	37.40	7.04	5.96	87.00
Co/ZrO_2-A	13.94	2.94	3.56	93.50
Co/ZrO_2-V	20.57	1.77	1.97	96.26

[a]The data of the seventh day (stable for 72 h) were selected. Reaction condition: T=200 °C, P =2 MPa, GHSV= 1000 h^{-1}, H_2/CO = 2.

Table S4 The FTS performance of the representative Co-based catalysts.

Catalyst	CO Conv. (%)	Hydrocarbon Sel. (%)			Reaction condition	Ref.
		CH_4	C_2-C_4	C_{5+}		
Co@C-100	76.1	11.4	11.3	77.3	T=220 °C, 2 MPa, H_2/CO=2, GHSV=1000 h^{-1}	1
Co@SiO_2-873	15.8	5.3	4.2	90.5	483 K, 2 MPa, and H_2/CO= 1, WHSV=24,000 mL/(g·h)	2
Co/Al_2O_3-15CN	71.3	10.3	11.9	77.8	225 °C, 2 MPa, H_2/CO = 2, GHSV = 1000 h^{-1}	3

ASC-15	50.5	6.3	5.0	88.7	210 °C, 2 MPa, 1000 h^{-1}, $H_2/CO = 2$	4
12Co/α-Al_2O_3	42	7.73	4.16	85.39	230 °C, 2 MPa, 3.3 NL g^{-1} h^{-1}, H_2/CO = 2	5
15%Co/Al_2O_3S-che	35	10	-	-	220 °C, 2.0 MPa, $H_2/CO = 2$, 10,000 mL·g^{-1}·h^{-1}	6
15Co/AC-15	56.3	2.8	4.5	92.7	195 °C, 2 MPa, 1.05 L g^{-1} h^{-1}, $H_2/CO = 2$	7
Co/Al_2O_3-CAI	56.1	3.2	2.8	94.0	210 °C, 2 MPa, 1000 h^{-1}, $H_2/CO = 2$	8
CoOx/SiO_2-A#	56.39	10.13	8.56	81.31	220 °C, 2 MPa, 2000 h^{-1}, $H_2/CO/N_2$ = 16/8/1.	9
Co/RAl_2O_3-550	56.0	2.7	4.1	93.2	200 °C, 2 MPa, 1000 h^{-1}, $H_2/CO = 2$	10

Reference:

1. Y. Liu, B. Hou, C. Chen, L. Jia, Z. Ma, Q. Wang, D. Li, Carbon coated cobalt catalysts for direct synthesis of middle n-alkanes from syngas, Fuel, 2022, 327,124889.

2. X. Sun, A. I. Olivos Suarez, M. Meijerink, T. Deelen, S. Ould-Chikh, J. Zečević, K. P. de Jong, F. Kapteijn, J. Gascon, Manufacture of highly loaded silica-supported cobalt Fischer–Tropsch catalysts from a metal organic framework, Nat. Commun., 2017, 8(1), 1680.

3. S. Guo, C. Niu, Z. Ma, J. Wang, B. Hou, L. Jia, D. Li, A novel and facile strategy to decorate Al_2O_3 as an effective support for Co-based catalyst in Fischer-Tropsch synthesis, Fuel, 2021, 289, 119780.

4. Y. Liu, L. Jia, B. Hou, D. Sun, D. Li, Cobalt aluminate-modified alumina as a carrier for cobalt in Fischer–Tropsch synthesis, Appl. Catal. A: Gen., 2017, 530, 30-36.

5. S. Rane, Ø. Borg, J. Yang, E. Rytter, A. Holmen, Effect of alumina phases on hydrocarbon selectivity in Fischer–Tropsch synthesis, Appl. Catal. A: Gen., 2010, 388(1–2), 160-167.

6. M. Lu, N. Fatah, A. Y. Khodakov, Solvent-free synthesis of alumina supported cobalt catalysts for Fischer–Tropsch synthesis, J. Energy Chem., 2016, 25, 1001-1007.

7. M. Zhong, J. Wang, C. Chen, Z. Ma, L. Jia, B. Hou, D. Li, Incorporating silicon carbide nanoparticles into Al_2O_3@Al to achieve an efficient support for Co-based catalysts to boost their catalytic performance towards Fischer–Tropsch synthesis, Catal. Sci. Technol., 2019, 9, 6037.

8. Y. Liu, L. Li, J.F. Zhang, B. Hou, Fabrication of highly active and durable Co/Al_2O_3 Fischer–Tropsch catalysts via coordination-assisted impregnation strategy, Fuel, 2024, 375,132569.

9. L. Li, Y. Liu, J. Zhang, M. Xia, W. Ji, MOFs-assisted synthesis of robust and efficient cobalt-based Fischer–Tropsch catalysts, Fuel, 2022, 329,125481.

10. Q. Jiao, Y. Liu, R. Yu, L. Li, Anchoring metal cobalt species on defective alumina for enhanced catalytic performance in FT synthesis, New J. Chem., 2025, 49, 14373.